Editors' Suggestion

Beam intensity limitations in future multibend achromat light sources

I. Agapov and S. A. Antipov
Deutsches Elektronen-Synchrotron DESY, Notkestraße 85, 22607 Hamburg, Germany

(Received 19 May 2025; accepted 21 January 2026; published 13 February 2026)

We show that the emittance of fourth-generation 6 GeV machines such as PETRA IV is close to what is theoretically achievable due to beam intensity limitations from space charge and intrabeam scattering. By investigating these limitations, in particular their scaling with the bare lattice emittance and the beam energy, we argue that achieving further significant emittance reduction is only possible by increasing the beam energy. We show further that electron energy increase is also the most efficient path toward higher radiation brightness.

DOI: 10.1103/5hw4-3ggc

I. INTRODUCTION

The quest for higher photon beam brightness in light sources to advance a wide spectrum of experimental techniques has ushered in the so-called fourth generation of low-emittance ring designs based on multibend achromat (MBA) lattices [1]. Many of these machines have now become operational or will be constructed in the near future [2–6]. In this latest generation, a number of collective effects are encountered that have not manifested in third-generation light sources. For both low-energy and high-energy machines, intrabeam scattering (IBS) has a significant impact on equilibrium emittance, requiring mitigation by higher-harmonic cavities [7]. Additionally, the space charge (SC) tune shift cannot be neglected anymore. For fourth-generation light sources, it exceeds the synchrotron tune and leads to a variety of dynamic effects [8].

In this paper, we investigate these effects and their possible implications on further improvement of brightness. As analytical treatment of realistic low-emittance lattices appears impossible and practical lattice design to reach certain target parameters involves multiple trade-offs, we study these limitations through a mixture of analytical estimates and scaling of the hybrid six-bend achromat (H6BA) lattice [9,10], the latest concept in the multibend achromats, on which, for instance, the design of the PETRA IV facility is based. The lattice is representative of the asymptotic performance for high-energy (~6 GeV) MBA light source designs when pushing the multibend achromats toward further compactness. It should be noted that lower-energy, compact storage rings may employ different design strategies (e.g., distributed dispersion rather than discrete dispersion bumps). As shown later in Appendix B, similar results hold for other lattice concepts.

Our analysis shows that both space charge and IBS present severe limitations that prevent a significant emittance reduction beyond what is currently achieved. These effects are mitigated by increasing the electron beam energy, which is also the most effective way to enhance the radiation brightness. At the same time, impedance-driven collective effects (e.g., microwave, coupled-bunch instabilities) might further constrain beam intensity and brightness. Discussion of collective effects and their mitigation goes beyond the scope of the present study.

II. NATURAL EMITTANCE SCALING

First, let us recall the well-known formulae for equilibrium beam parameters in electron storage rings [11,12]. The natural rms emittance, energy spread, and bunch length are

$$\begin{aligned} \epsilon_0 &= C_q \gamma^2 \frac{I_5}{j_x I_2}, \\ \sigma_\delta^2 &= C_q \gamma^2 \frac{I_3}{j_z I_2}, \\ \sigma_z &= \frac{\alpha_C c}{\omega_s} \sigma_\delta, \end{aligned} \tag{1}$$

where $C_q \approx 3.8 \times 10^{-13}$ m, α_C is the momentum compaction factor, ω_s the angular synchrotron frequency, c the speed of light, and γ the relativistic factor. The so-called radiation integrals along the circumference are defined as

$$\begin{aligned} I_2 &= \oint \frac{1}{\rho^2} ds, \\ I_3 &= \oint \frac{1}{|\rho|^3} ds, \\ I_4 &= \oint \frac{\eta_x}{\rho} \left(\frac{1}{\rho^2} + 2k_1 \right) ds, \\ I_5 &= \oint \frac{\mathcal{H}_x}{|\rho|^3} ds, \end{aligned} \tag{2}$$

where $\mathcal{H}_x = \gamma_x \eta_x^2 + 2\alpha_x \eta_x \eta_{px} + \beta_x \eta_{px}^2$ is the horizontal dispersion invariant. The partition numbers $j_x = 1 - I_4/I_2$, $j_y = 1$, and $j_z = 2 + I_4/I_2$ are influenced primarily by focusing in the combined-function magnets and indicate how the damping is shared between planes, with the damping times $\tau_{x,y,z}$ and rates $\alpha_{x,y,z}$ defined as

$$\tau_{x,y,z} = \alpha_{x,y,z}^{-1} = \frac{2}{j_{x,y,z}} \frac{E_0}{U_0} T_0, \tag{3}$$

where T_0 is the revolution period, E_0 the beam energy, and U_0 is the energy loss per turn:

$$U_0 = \frac{C_\gamma}{2\pi} E_0^4 I_2, \tag{4}$$

with $C_\gamma \approx 8.8 \times 10^{-5}\ \mathrm{m/GeV^3}$.

We will consider a machine of fixed circumference, for example, that of PETRA (2304 m), and the potential emittance reduction through low-emittance lattice beyond what will be achieved at PETRA IV. For all multibend achromat lattices, including those using damping wigglers, I_2 is relatively independent of the machine optics. The biggest effect of emittance reduction is achieved through a decrease of the I_5 integral by stronger focusing. The I_3 integral is also only weakly dependent on the choice of optics, and the equilibrium energy spread becomes a function of energy mostly. Bunch length is reduced for low-emittance lattices as it is proportional to the momentum compaction.

Emittance reduction is usually achieved by increasing the number of bends and focusing elements in a cell of fixed length, for example, by going from the double-bend achromat (DBA) to the seven-bend achromat (7BA or H7BA) cell, e.g., Refs. [12,13]. Analytical expressions exist that describe emittance scaling with the number of magnets per cell for standard arrangements such as FODO or theoretical minimum emittance cell. However, a practical design does not follow such cell structures, since additional constraints such as space for insertion devices should be satisfied. An example of such a design is the H6BA cell adopted for PETRA [9,10]. Since simple closed-form analytical expressions for optical functions in an MBA optics are not readily available, we will study the scaling of parameters based on the scaling of the H6BA cell of PETRA IV (Fig. 1). Such scaling is achieved by reducing all element lengths by a factor f, increasing quadrupole strength by f^2, and sextupole strength by f^4 to have the same corrected chromaticity. We ignore the higher order multipole (octupole) scaling as they are not essential for this analysis. Thus our scaling is equivalent to reducing the cell length by a *scaling factor f*.

While a realistic design of a smaller emittance lattice will certainly not follow this path, the achieved values of beta functions, dispersion invariant $\mathcal{H}$, and radiation integrals will necessarily be similar to an H6BA cell scaled to achieve similar emittance values, and the scaling factor has to be understood as a parametrization of possible emittance reduction.

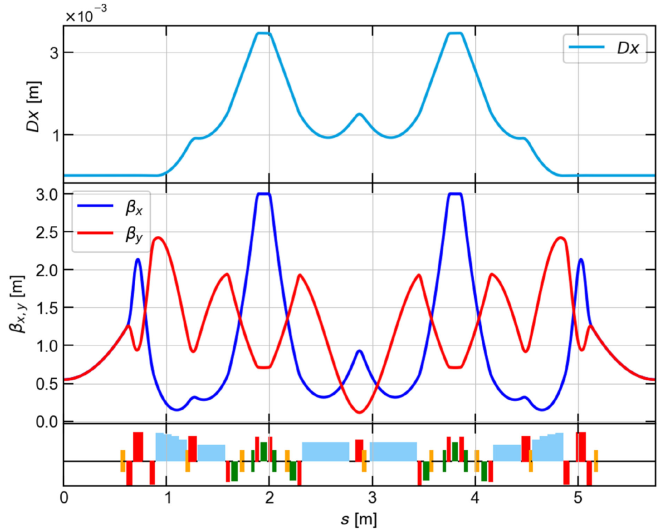

FIG. 1. Scaled H6BA cell of PETRA IV reduced in length by a factor $f = 4$.

Figure 2(a) shows emittance as a function of scaling parameter for various beam energies, calculated using Eqs. (1) and (2). Note that in practice emittance can be further reduced by damping wigglers (e.g., as it will be done in PETRA IV). The choice of damping wiggler parameters is usually done such that equilibrium bunch length and energy spread are minimally affected, but emittance is reduced via increase in I_2. I_2, as mentioned before, is independent of lattice scaling. It does not affect the space charge limitations, but can be used to mitigate the

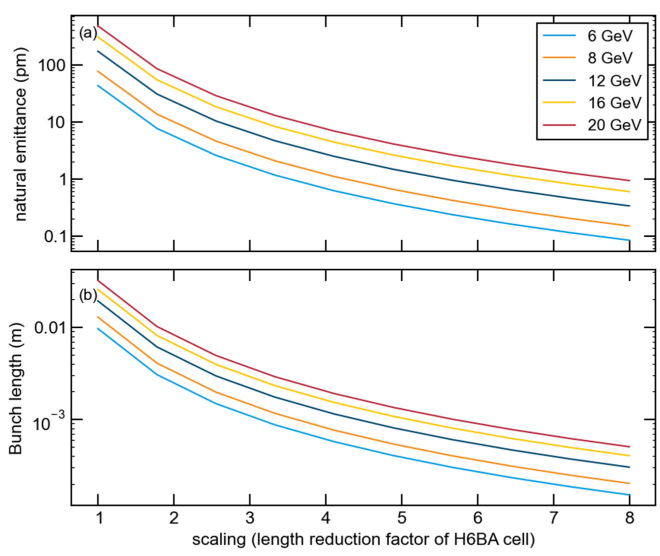

FIG. 2. Scaling with energy and cell length of natural emittance (a) and bunch length (b).

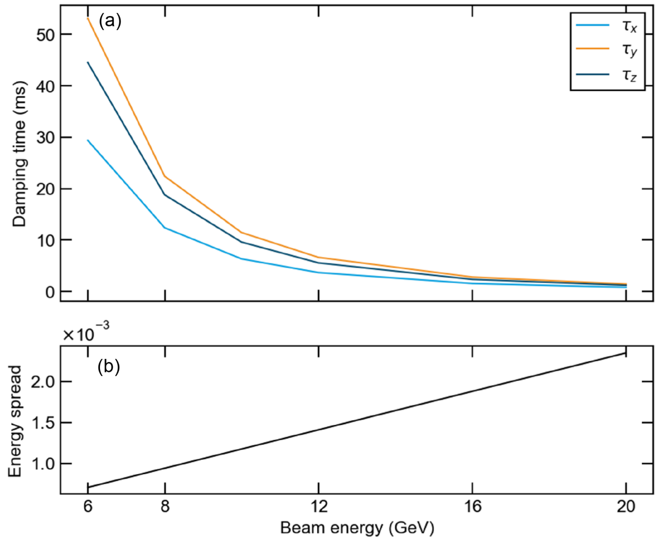

FIG. 3. Damping times (a) and energy spread (b) vs beam energy. There is no dependence on lattice scaling.

intrabeam scattering effect to some extent, e.g., by a factor of 2 in the case of PETRA IV, at the cost of increased radiation losses and rf power. We briefly discuss their effect on the H6BA lattice case in Appendix B. In practice, the use of damping wigglers is usually restricted by available space. Its efficiency is limited to machines constructed in old collider tunnels, where sections unused by insertion devices are available, or greenfield projects such as NSLS-II [14], where they could be foreseen from the start.

Figure 2(b) shows the bunch length scaling with energy and lattice scaling. Figure 3 shows the dependencies of the damping times and the equilibrium energy spread on the beam energy, computed using Eqs. (3) and (4). They are both independent of the lattice scaling.

Here an implicit dependency of synchrotron frequency on the lattice parameters via momentum compaction α_C has been removed by fixing the synchrotron frequency at 1 kHz. An alternative assumption could be that the bunch length remains constant, which would however imply that the synchrotron frequency would approach zero when emittance is reduced, which is detrimental for collective stability. Both limiting cases are examined later numerically, showing minor differences in achievable emittances. Choice of rf parameters for optimal bunch lengthening should be carefully addressed in practice.

III. BEAM INTENSITY SCALING

A. Space charge estimates

Typically, SC effects are most prominent in the frontier high-intensity hadron machines and their injectors, while electron rings benefit from the much smaller particle mass as the SC interaction decreases with the Lorentz factor. Yet, the SC effects have already been found important in the linear collider damping rings where a combination of a relatively low beam energy and a small emittance makes SC interaction significant [15–18]. State-of-the-art light sources also share this combination, as pointed out in [8].

The Coulomb interaction between the particles will change their natural frequencies of oscillation around the reference orbit, causing the so-called space charge tune shift. In the linear model the incoherent tune shift of a Gaussian bunch is (see e.g., Ref. [19])

$$\Delta\nu_{x,y}^{\mathrm{SC}} = -\frac{N r_e C}{(2\pi)^{3/2}\gamma^3\sigma_z}\left\langle\frac{\beta_{x,y}}{\sigma_{x,y}(\sigma_x+\sigma_y)}\right\rangle, \tag{5}$$

where N is the number of particles per bunch, $\sigma_{x,y,z}$ are the rms horizontal, vertical, and longitudinal beam sizes, γ is the Lorentz factor, $\beta_{x,y}$ are the transverse Twiss optics functions, and $\langle\ldots\rangle$ denotes averaging over the ring circumference C. $r_e = e^2/m_e c^2 \approx 2.8\times10^{-13}$ cm (in cgs units) stands for the classical electron radius and c is the speed of light. For realistic light source lattices and flat beams (the betatron coupling ratio $\kappa \ll 1$) this formula can be further simplified and an estimate of the tune shift (here in the vertical y plane, where it is usually the largest) becomes (see Appendix A for derivation)

$$\Delta\nu_y^{\mathrm{SC}} \approx -\frac{1}{4\kappa}\frac{N r_e C}{(2\pi)^{3/2}\gamma^3\sigma_z\epsilon_x}. \tag{6}$$

As SC drives the incoherent tunes to cross the integer resonance it establishes a hard, first-principle limit on the maximum beam intensity that can be stored in the ring. One can impose that $|\Delta\nu_y^{\mathrm{SC}}| \lesssim 0.5$. Then, defining the peak beam brightness as $B = 2I/\pi^2\epsilon_x\epsilon_y = 2I/\pi^2\epsilon_x^2\kappa$, where I stands for the peak bunch current, its achievable upper limit in any light source becomes

$$B\times\epsilon_x \lesssim 8\gamma^3 I_A/\pi C, \tag{7}$$

where $I_A = m_e c^3/e \approx 17$ kA is the Alfven current. Note that this limit is independent of the details of the focusing lattice and only depends on two factors: the beam energy and the ring circumference. For our 6 GeV 2.3-km-long PETRA IV example with $\epsilon_x = 20$ pm one obtains that the brightness cannot exceed $B < 1.5\times10^{24}$ A/m^2. For the PETRA IV circumference, bunch length, and 6 GeV energy, the space charge effect would limit the emittance to about 5–10 pm [20].[1] The scaling of SC implies that achieving emittances of 1 pm and below should be possible by raising the energy to about 10 GeV.

B. IBS estimates

With damping rate α and quantum diffusion rate D, the beam distribution evolution is described by the

[1]The exact limit depends on bunch length and coupling ratio.

Fokker-Planck equation for action J in each of the x, y, z coordinates

$$\partial_t f(J) = \alpha \partial_J f(J) + D \partial_{JJ} f(J). \tag{8}$$

If one looks for a stationary solution in the form $f_0 e^{-J/\epsilon}$, where ϵ is the equilibrium emittance, one gets $\epsilon = D/\alpha$. Now, the damping rate is the sum of synchrotron radiation damping and IBS-induced growth, $\alpha = \alpha_{\mathrm{SR}} - \alpha_{\mathrm{IBS}}$, so we can write the following

$$\epsilon = \frac{D/\alpha_{\mathrm{SR}}}{1 - \alpha_{\mathrm{IBS}}/\alpha_{\mathrm{SR}}} = \frac{\epsilon_0}{1 - \alpha_{\mathrm{IBS}}/\alpha_{\mathrm{SR}}}, \tag{9}$$

where ϵ_0 is the equilibrium emittance without taking IBS into account [21–23]. It is clear that for the beam to achieve equilibrium one should have $\alpha_{\mathrm{IBS}} < \alpha_{\mathrm{SR}}$. For IBS growth rate not exceeding synchrotron damping, the equilibrium emittance can be found numerically by solving Eq. (9) with emittance-dependent IBS growth rates given by [24]

$$\begin{aligned} \alpha_{x,y}^{\mathrm{IBS}} &\approx \frac{r_e^2 c N L_C}{16\gamma^3 \epsilon_{x,y}^{\frac{7}{4}} \epsilon_{y,x}^{\frac{3}{4}} \sigma_z \sigma_p} \left\langle \frac{\mathcal{H}_{x,y} \sigma_H g(x)}{(\beta_x \beta_y)^{\frac{1}{4}}} \right\rangle, \\ \alpha_p^{\mathrm{IBS}} &\approx \frac{r_e^2 c N L_C}{16\gamma^3 \epsilon_x^{\frac{3}{4}} \epsilon_x^{\frac{3}{4}} \sigma_z \sigma_p^3} \left\langle \frac{\sigma_H g(x)}{(\beta_x \beta_y)^{\frac{1}{4}}} \right\rangle, \end{aligned} \tag{10}$$

where L_C is the Coulomb log and $g(x) \approx 2x^{0.021 - 0.044 \ln x}$. Here $\mathcal{H}_{x,y}$ are the dispersion invariants in the horizontal and the vertical plane accordingly and σ_p is the relative rms momentum spread; the other parameters of the model are defined as

$$\begin{aligned} x &= b_x/b_y, \\ b_{x,y} &= \sigma_H/\gamma \times \sqrt{\beta_{x,y}/\epsilon_{x,y}}, \\ \sigma_H &= \sqrt{\sigma_p^{-2} + \mathcal{H}_x/\epsilon_x + \mathcal{H}_y/\epsilon_y}. \end{aligned} \tag{11}$$

With increasing scaling factor, the equilibrium emittance and bunch length decrease (Fig. 2). This, in turn, enhances the IBS effect and reduces the ratio of SR damping rate to IBS growth rate (Fig. 4) until at a certain point it becomes 1. Beyond that point, the equilibrium emittance is fully dominated by IBS. This IBS threshold is increased and smaller equilibrium emittances can be reached at higher beam energies.

C. Minimum achievable emittance

In order to find the equilibrium emittance in the presence of strong IBS, we solved for an equilibrium between IBS, SR, and quantum excitation (QE) given by Eq. (9) numerically, accounting for both the longitudinal and the transverse degrees of freedom. In the latter, we assumed that $\mathcal{H}_y \approx 0$ and the vertical IBS growth rate can be neglected, with the vertical emittance governed by a small betatron coupling ratio κ. The bunch length is strongly influenced by the choice of rf parameters, including the harmonic rf and longitudinal impedance. For example, while the natural zero-current bunch length of PETRA IV is ~7 ps, these effects increase it to about 40 ps for a 1 nC bunch in brightness mode and to 65 ps for an 8 nC bunch in timing mode. Thus, we assumed that the natural bunch length is further increased by a factor of 10 for the calculations. Bunch charge of 1 nC for the standard brightness mode fill pattern was used.

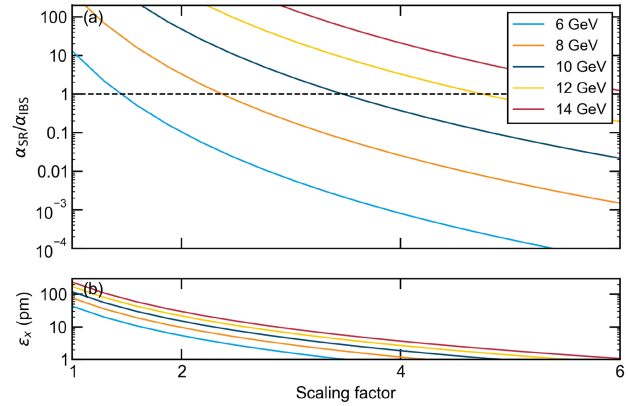

FIG. 4. Evolution of SR and IBS rates (a) and emittance (b) as a function of the lattice scaling factor f. As emittance decreases with scaling, the IBS rate exceeds the SR (dashed line) limiting further emittance reduction. Coupling $\kappa = 0.1$.

The resulting emittance landscape for different energies and lattice scalings is presented in Fig. 5. As expected, emittance increases with energy and decreases with the scaling factor up to a point where it becomes limited by IBS. Beyond this point, a further increase of the scaling factor only slightly improves the emittance. For example, for a 6 GeV lattice and a moderate to high coupling of 0.1–0.5, the minimum emittance reaches 10 pm at a scaling factor of about 2.5 (down from the nominal of ~40 pm for an H6BA), and a further reduction is possible only with a significant increase of the scaling.

Examining Fig. 5 further, one can notice that there seem to be optimal combinations of scale and energy for any given target emittance: the corner points on curves of equal emittance. They represent local minima of emittance with respect to variation of energy and scale: the local minimum of emittance with respect to variation of energy and scale.

Further, one can see in Fig. 5 the space charge exclusion area. As discussed above, it arises from crossing of the integer resonance by the SC tune spread and can be estimated using Eq. (7). The SC effectively prohibits reaching very small emittances and dictates that a decrease of the beam emittance must be accompanied by an increase of the beam energy.

Finally, we can depict the expected equilibrium energy spread reachable under IBS as it is an important parameter, relevant for photon science users. Figure 6 presents our

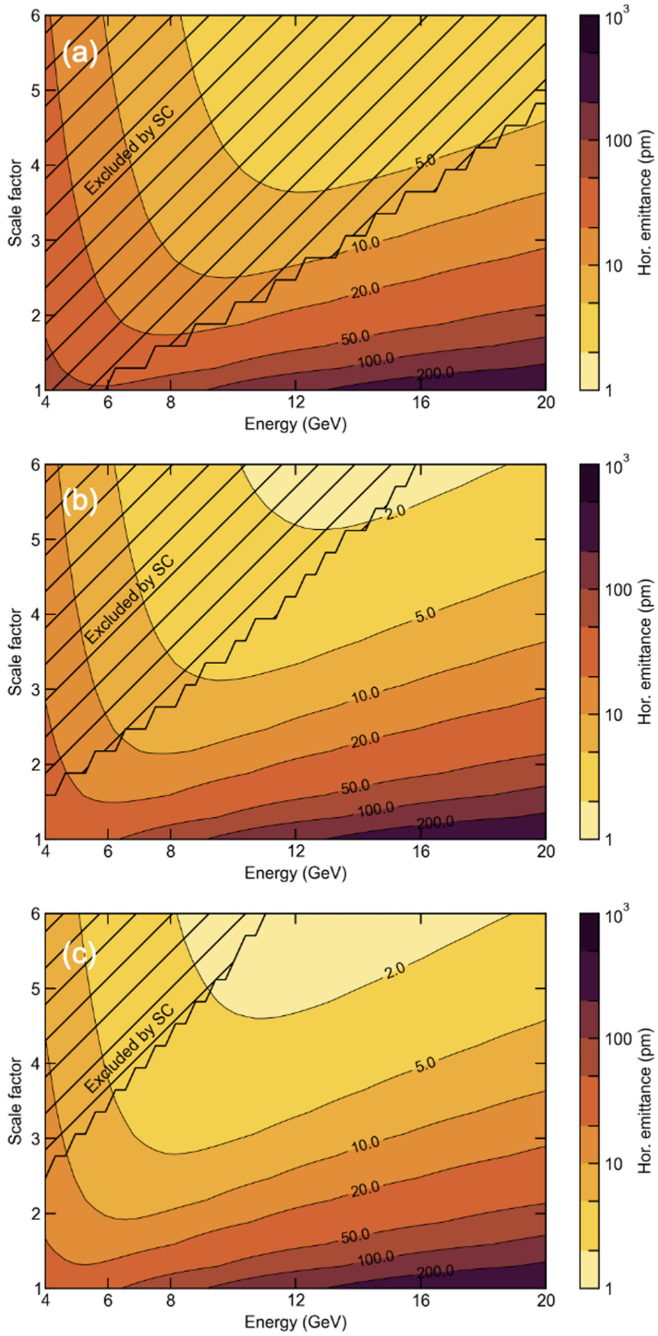

FIG. 5. Achievable emittances as a function of beam energy and lattice scaling factor f for different couplings: $\kappa = 0.01$ (a), $\kappa = 0.1$ (b), and $\kappa = 0.5$ (c). Equilibrium emittance is defined by the balance of SR, QE, and IBS. A factor of 10 bunch lengthening by a harmonic rf system is assumed. The hatched area denotes the parameter space unavailable due to the space charge tune spread, $|\Delta\nu_y^{\mathrm{SC}}| > 0.5$. Bunch charge is 1 nC.

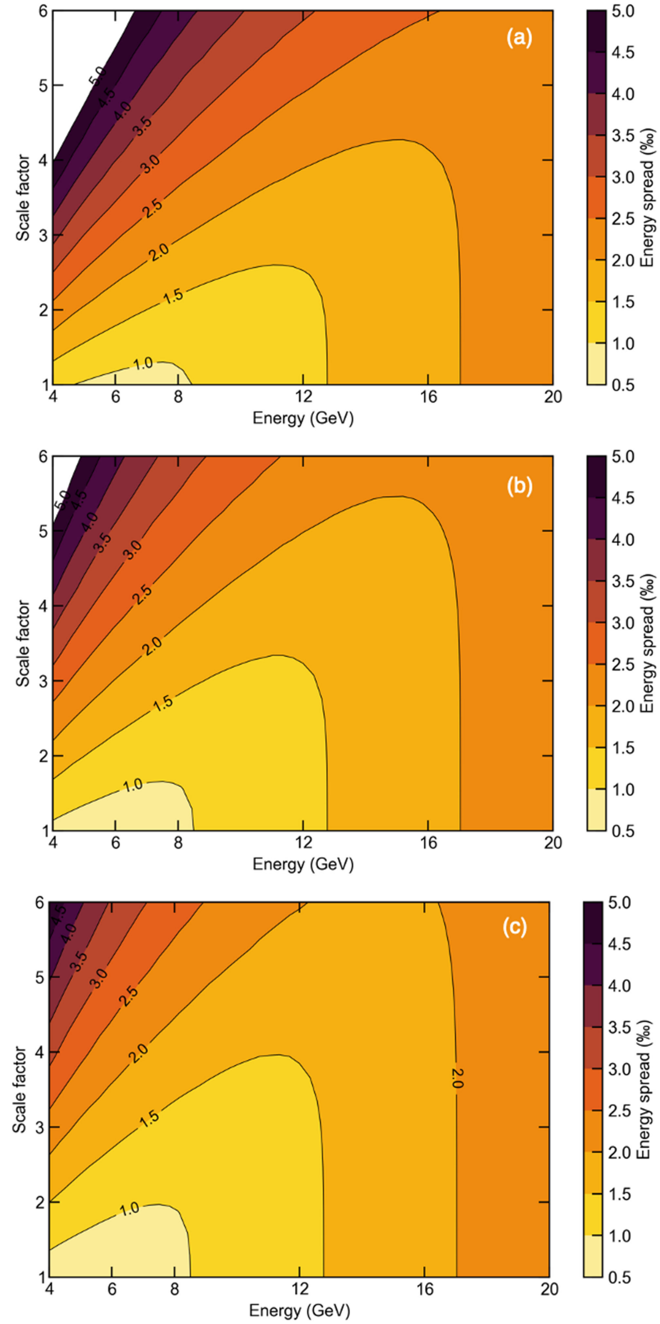

FIG. 6. Achievable rms energy spreads as a function of beam energy and lattice scaling factor f for different coupling ratios: $\kappa = 0.01$ (a), $\kappa = 0.1$ (b), and $\kappa = 0.5$ (c). Equilibrium energy spread is defined by the balance of SR, QE, and IBS. A factor of 10 bunch lengthening by a harmonic rf system is assumed. Bunch charge is 1 nC.

numerical findings. In the region not dominated by SC, the equilibrium energy spread increases steadily with the energy and does not exhibit a strong dependence on the scaling.

As our assumption on the bunch length might have been overly pessimistic, we also examined another "extreme" scenario where the bunch length is kept constant across all cases, at 40 ps. This results only in a minor difference in achievable emittances (Fig. 7). Similarly to Fig. 5, the upper-left part of the parameter space is excluded by SC. Notably, the choice of bunch length affects the limits of the SC-dominated region with longer bunches allowing smaller emittances to be reached at large scaling factors.

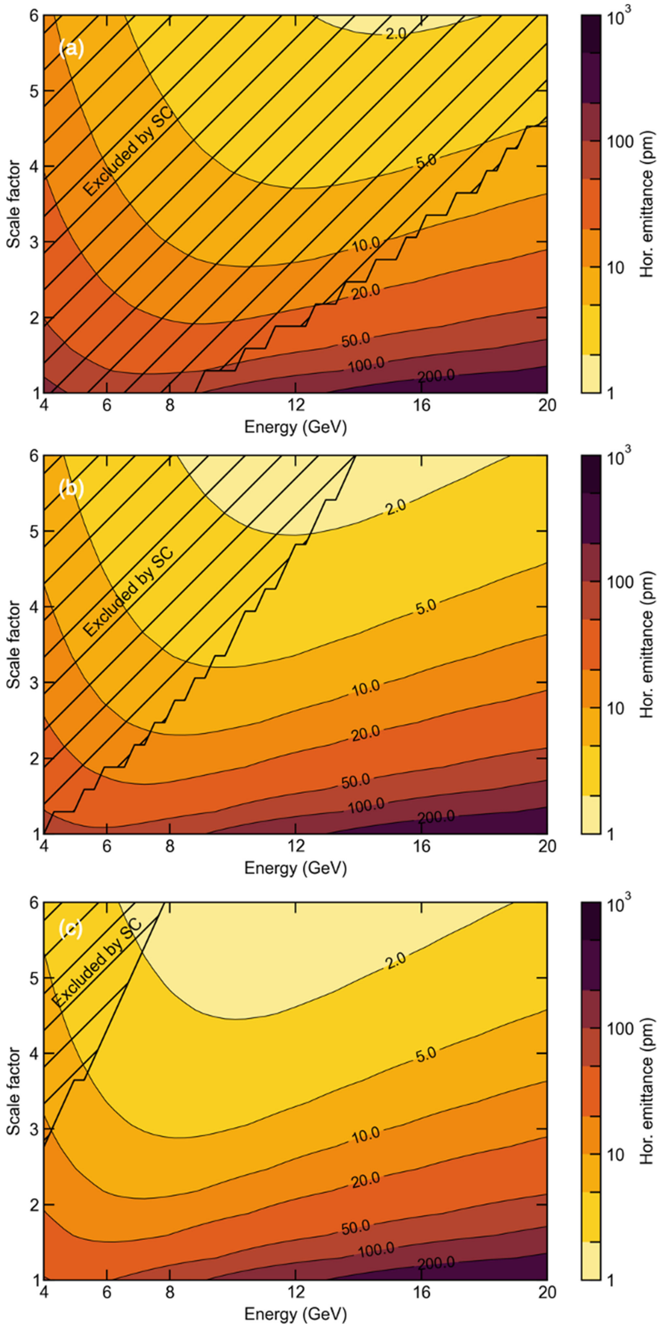

FIG. 7. Achievable emittances as a function of beam energy and lattice scaling factor f for different couplings: $\kappa = 0.01$ (a), $\kappa = 0.1$ (b), and $\kappa = 0.5$ (c). Equilibrium emittance is defined by the balance of SR, QE, and IBS. Bunch stretching by a harmonic rf system to 40 ps across all cases is assumed. The hatched area denotes the parameter space unavailable due to the space charge tune spread, $|\Delta\nu_y^{\mathrm{SC}}| > 0.5$. Bunch charge is 1 nC.

Examining the IBS growth rates, Eq. (10) reveals that they are primarily functions of emittance and energy. At the same time, the SR damping time is independent of emittance and circumference, and decreases with energy. This implies that our scalings should also hold, in principle, for smaller machines, while small emittances might be harder to achieve there in practice (see Appendix B). From the point of view of space charge, which depends strongly on the energy and increases with circumference, a higher beam energy and a smaller circumference are preferable.

D. Comment on other effects

First, let us consider the Touschek lifetime, which depends strongly on beam energy and momentum acceptance:

$$T_{\mathrm{touschek}} \propto \gamma^2 \delta_{\mathrm{acc}}^3. \tag{12}$$

In the state-of-the-art light sources, such as PETRA IV, this lifetime may reach ∼100 h. It will further increase with beam energy. At the same time, emittance reduction might lead to a decrease in momentum acceptance. For a practical lattice, the latter should remain significantly larger than the rms energy spread (Fig. 6).

For both single and multibunch instabilities, the scaling of thresholds is usually proportional to energy. For example, the single-bunch transverse instability limit can be quantified by the TMCI threshold

$$I_{\mathrm{th}} \propto \frac{\gamma \omega_s \sigma_z}{\beta_{x,y} Z_T}, \tag{13}$$

where Z_T is the impedance sampled at harmonics of revolution and synchrotron frequency. In practice, this limit is significantly increased with chromaticity, and does not manifest itself unless operating the machine in a mode with few high-charge bunches. At PETRA IV, for the 2 ns uniform bunch filling, the single-bunch intensity is roughly a factor of 50 smaller than the threshold bunch current. A similar scaling is valid for coupled-bunch instabilities. In general, however, coupled-bunch instabilities do not limit machine performance when feedback systems are employed.

Machine impedance is strongly dependent on choice of apertures, and, in the case of rf, on the resonator frequency and technology. The scaling of geometric impedance is with the inverse square of the vacuum chamber dimension, b^{-2}, whereas the resistive wall contribution scales with the cube, b^{-3}. The detailed investigation of impedance goes beyond the present discussion. But both single- and coupled-bunch instability scalings are such that the intensity thresholds generally improve with beam energy and are not limiting the machine performance unless the impedance is drastically increased. This can be a limitation in practice if high-gradient magnets and high-voltage rf require significantly reducing the vacuum chamber dimensions and increasing the rf frequency.

IV. RADIATION BRIGHTNESS SCALING

A relevant figure of merit for the undulator radiation is its peak photon beam brightness, commonly measured in units of photons/s mm^2 mrad^2 (0.1% bandwidth), which can be approximated as [25,26]

$$\mathcal{B}_{ph.pk} = \frac{\mathcal{F}_n}{(2\pi)^2 \sigma_{T,x}\sigma_{T,y}\sigma_{T,x'}\sigma_{T,y'}}, \tag{14}$$

where $\mathcal{F}_n$ is the spectral flux, σ_T include the photon contribution to the effective beam size, $\sigma_{T,x} = \sqrt{\sigma_x^2 + \sigma_r^2}$ and $\sigma_{T,x'} = \sqrt{\sigma_{x'}^2 + \sigma_{r'}^2}$ (and similarly for the y plane), $\sigma_r = \sqrt{\lambda L_u}/4\pi$. Effect of emittance and energy spread on brightness and coherence is discussed in more detail in [27,28]. Let us assume operating close to a diffraction limit, such that

$$\epsilon_x \sim \epsilon_D = \frac{\lambda}{4\pi}. \tag{15}$$

Then one may assume that $\sigma_x \sim \sigma_r$ and $\sigma_{x'} \sim \sigma_r'$. So, for the sake of an order of magnitude estimate, we can write the peak photon brightness as

$$\mathcal{B}_{ph.pk} \sim \frac{1}{2\pi\sigma_x\sigma_y}\frac{\partial^2\mathcal{F}_n}{\partial\Theta\partial\psi} \propto \frac{\gamma^2 I}{\epsilon_x^2\kappa} = \frac{16\pi^2\gamma^2 I}{\lambda^2\kappa}, \tag{16}$$

where κ is a fixed transverse emittance coupling ratio $\kappa = \epsilon_y/\epsilon_x$. Note that the ratio of bunch current to the square of emittance, $I/\epsilon_x^2 \propto B$, the peak beam brightness, is fundamentally limited by space charge tune shift, as shown in Eq. (6). This means that the space charge tune shift poses a limit to how far one can push peak photon brightness for a given undulator technology.

Further factors have to be considered. First, the radiation wavelength (first harmonic) of an undulator is

$$\lambda = \frac{\lambda_u}{2\gamma^2}\left(1 + \frac{K^2}{2}\right), \tag{17}$$

where $K = eB\lambda_u/2\pi m_e c$. Increasing the beam energy while keeping the same radiation wavelength requires an increase in the undulator parameter K or the undulator period λ_u. Both will result in broadening of radiation spectrum, which is not desirable. Moreover, the brightness improvement with emittance is limited by the diffraction limit on emittance. For a typical radiation energy of 10 keV (or a wavelength of 1.2 Å), Eq. (15) yields the diffraction limit of about 10 pm. Decreasing emittance beyond that for this wavelength does not improve brightness. Simultaneous increase in electron beam energy and reduction in emittance would allow to dramatically extend both the diffraction-limited wavelength and the achievable brightness using similar insertion devices. So, according to Eq. (16), a reduction from 20 pm emittance to 2 pm and increasing energy to 18 from 6 GeV leads to an order of magnitude in photon energy reach and diffraction limit, and in nearly 3 orders of magnitude in peak brightness.

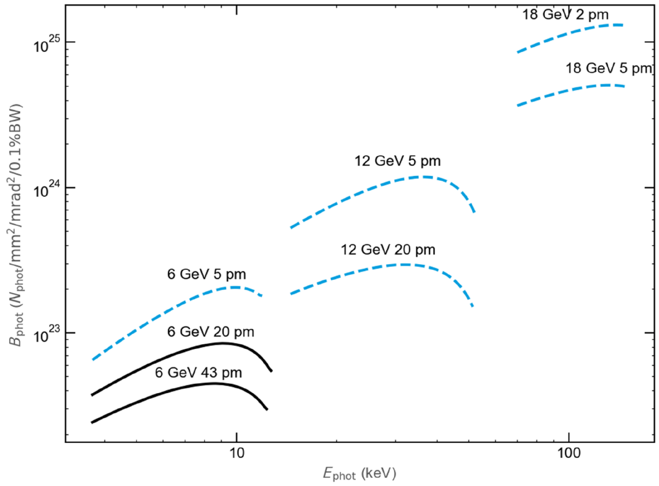

FIG. 8. Radiation brightness for various scenarios. For all curves, insertion device length is $L = 4.5$ m, $\beta_x = \beta_y = 2$ m, $\kappa = 0.1$. For 6 GeV: $\lambda_u = 2.3$ cm, $\sigma_p = 0.7 \times 10^{-3}$ for 43 pm emittance, and $\sigma_p = 1 \times 10^{-3}$ for 20 pm emittance. For 12 GeV: $\lambda_u = 2.3$ cm, $\sigma_p = 1.5 \times 10^{-3}$. For 18 GeV: $\lambda_u = 1.3$ cm, $\sigma_p = 2 \times 10^{-3}$.

Brightness for given undulator and beam parameters can be found more precisely with the help of specialized codes. Calculations of brightness with SPECTRA [29] for several scenarios of emittance reduction and energy increase are shown in Fig. 8. There the solid black curves represent the parameters achievable at PETRA IV with and without taking damping wigglers into account. Even a reduction to 5 pm emittance, which is already beyond the space charge and IBS limitation (Fig. 5), would increase the brightness by no more than a factor of 3 for a typical insertion device with the parameters listed in the caption of Fig. 8. Other dashed curves represent hypothetical scenarios for simultaneous increase of beam energy and decrease of emittance based on the H6BA scaling. At about 18 GeV, the theoretically achievable emittance of 2 pm (cf. Fig. 5) would result in simultaneous increase of brightness by more than 2 orders of magnitude and of photon energy reach by 1 order of magnitude.

V. DESIGN IMPLICATIONS FOR HIGH-ENERGY LOW-EMITTANCE SOURCES

The dramatic increase of brightness while pursuing lower-emittance lattices for higher beam energy comes at a cost. For a moderate scaling factor of 2 in the H6BA PETRA IV cell and an increase of energy from 6 to 8 GeV, an emittance of about 10 pm can be achieved (see Fig. 5). Assuming usage of permanent magnet technology and reducing spacing between magnets such that the sextupoles and quadrupoles could be made twice longer compared to the resistive magnet design, we would arrive at quadrupole gradients of about 300–400 T/m, which is technically possible with permanent magnets [30], and sextupole strength of about 80 000 $\mathrm{T/m^2}$, which is beyond the current technological capabilities. A novel lattice concept beyond hybrid multibend achromat is required for chromaticity compensation in this case, with possibly more distributed sextupole compensation. Both vacuum pumping and impedance issues will become more prominent problems in such designs.

Independent of the approach for lowering the emittance further, dynamic aperture limitations will become more dramatic, with values possibly below 1 mm. A combination of novel injection schemes with future low-emittance injectors, such as the LPA injector being developed at DESY [31,32], would allow such machines to operate efficiently.

HOM-damped normal-conducting cavities used in light sources would be inefficient to cope with an increased voltage required to compensate synchrotron radiation losses at a higher beam energy. Here, superconducting cw cavities can be employed more efficiently [33,34].

VI. CONCLUSION AND OUTLOOK

We analyzed potential obstacles on the path toward further emittance reduction in MBA lattices and showed that space charge effects and IBS present a fundamental limitation on the way to considerable emittance reduction beyond the state-of-the-art synchrotron light sources. So, for a machine at 6 GeV with a ca. 2 km circumference, emittances below about 5 pm are practically unreachable unless the beam energy is raised. This limitation of emittance naturally translates to the photon brightness, where a significant improvement without raising the beam energy is impossible. On the other hand, increasing the energy from 6 to 16–18 GeV would open a completely new field of opportunities, increasing the brightness by more than two and the photon spectral reach by 1 order of magnitude. Technological limitations stand in the way of achieving this improvement with the known multibend achromat lattice concepts, and further R&D into design of low-emittance lattices is required.

Within our model, the fundamental space-charge and IBS limits are independent of the overall machine circumference. Yet, in general, smaller emittances are more accessible at larger machines. This makes photon science applications an appealing complementary option to the high energy physics program at the Future Circular Collider complex [35]. There an emittance of about 1–2 pm could be reached in its 20 GeV, 90 km circumference booster with standard technology before encountering intensity limitations.

ACKNOWLEDGMENTS

We thank Gianluca Geloni for cross-checking the brightness calculations, Frank Zimmermann for discussions concerning FCC booster parameters, and Reinhard Brinkmann for carefully reading the manuscript and making useful suggestions for improvement.

DATA AVAILABILITY

The data are not publicly available. The data are available from the authors upon reasonable request.

APPENDIX A: SPACE CHARGE TUNE SHIFT APPROXIMATION FOR LIGHT SOURCES

Consider a typical scenario of a machine operating with flat beams, $\sigma_y \ll \sigma_x$, then the largest tune shift occurs in the vertical, y plane. Further, assume that the ring is designed with a low-emittance approach in mind and the dispersion contributions to the beam size are, on average, small. Then the beam size is mostly governed by its emittance ϵ and one can substitute in Eq. (5) $\sigma_{x,y} = \sqrt{\beta_{x,y}\epsilon_{x,y}}$, arriving at

$$\Delta\nu_y^{\mathrm{SC}} = -\frac{N r_e C}{(2\pi)^{3/2}\gamma^3\sigma_z}\left\langle\frac{\beta_y}{\sqrt{\beta_y\epsilon_y}(\sqrt{\beta_x\epsilon_x}+\sqrt{\beta_y\epsilon_y})}\right\rangle. \tag{A1}$$

Introducing the coupling ratio as $\kappa = \epsilon_y/\epsilon_x$, the expression can be rewritten as

$$\Delta\nu_y^{\mathrm{SC}} = -\frac{N r_e C}{(2\pi)^{3/2}\gamma^3\sigma_z\epsilon_x\kappa}\left\langle\frac{\sqrt{\kappa}\sqrt{\beta_y/\beta_x}}{(1+\sqrt{\kappa}\sqrt{\beta_y/\beta_x})}\right\rangle, \tag{A2}$$

and for small κ, the term in the brackets is approximately

$$\left\langle\frac{\sqrt{\kappa}\sqrt{\beta_y/\beta_x}}{(1+\sqrt{\kappa}\sqrt{\beta_y/\beta_x})}\right\rangle \approx \left\langle\sqrt{\kappa}\sqrt{\frac{\beta_y}{\beta_x}}\left(1-\sqrt{\kappa}\sqrt{\frac{\beta_y}{\beta_x}}\right)\right\rangle. \tag{A3}$$

The last product of a type $p\times(1-p)$ is well known. As long as $0 < p < 1$, it cannot exceed 1/4. Therefore, we can replace the average with its upper limit, 1/4. With this simplification, the final estimate of the vertical tune shift becomes

$$\Delta\nu_y^{\mathrm{SC}} \approx -\frac{1}{4\kappa}\frac{N r_e C}{(2\pi)^{3/2}\gamma^3\sigma_z\epsilon_x}. \tag{A4}$$

The last approximation holds in a large range of coupling parameters for real-world accelerator lattices, as seen in Fig. 9, where it is tested for ESRF-EBS and PETRA IV HMBA lattices, as well as for DBA lattices of SOLEIL and PETRA III. The error of the approximation is within 25% for coupling ratios between 0.1 and 0.4. The formula above only applies to small coupling ratios and has to be modified slightly for the case of $\kappa \sim 1$ [20], but the general scaling remains the same.

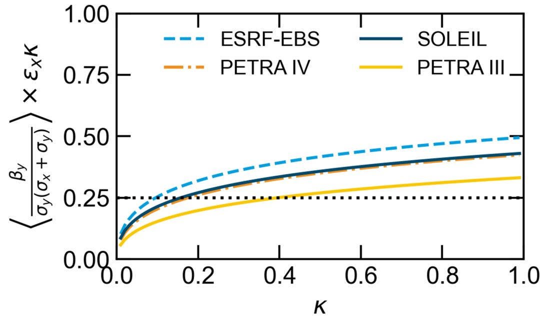

FIG. 9. A constant 0.25 (dotted line) provides a reasonable estimate for real-world light source lattices in a wide range of couplings κ [20].

In order for the particle motion to be stable, this tune shift must never cross an integer resonance. Considering that the light sources typically operate with their fractional tunes below 0.5 one can assert $|\Delta\nu_y^{\mathrm{SC}}| \lesssim 1/2$. Then introducing the peak beam brightness as $B = 2I/\pi^2\epsilon_x\epsilon_y = 2I/\pi^2\epsilon_x^2\kappa$, where I stands for the peak bunch current, one obtains Eq. (7).

APPENDIX B: EMITTANCE SCALING FOR SOME OTHER LATTICE TYPES

To check the generality of our approach, we performed our analysis on two additional low-emittance synchrotron lattices. In both cases, the results are consistent with our previous findings. The first one is the PETRA IV H6BA lattice with damping wigglers. We modeled the effect of wigglers by modifying the I_2 integral and adjusting the beam parameters (i.e., emittance, damping partition numbers, SR damping times) accordingly. In the absence of IBS, the wigglers reduce the horizontal emittance from 43 to 20 pm. In the presence of IBS, the equilibrium emittance of the unscaled lattice at 6 GeV is 29 pm, which is reasonably close to the 24 pm value obtained in tracking simulations with IBS and impedance effects included [9], given all the approximations of our model. In the presence of IBS and space charge, the landscape is qualitatively similar to the no-wiggler case. The equilibrium emittance decreases when shortening the cell length up to a certain point, where IBS makes further emittance reduction with cell scaling inefficient (Fig. 10). As in the no-wiggler case, there is an optimum scale of the cell for each energy. The smaller emittance, achieved with damping wigglers, makes

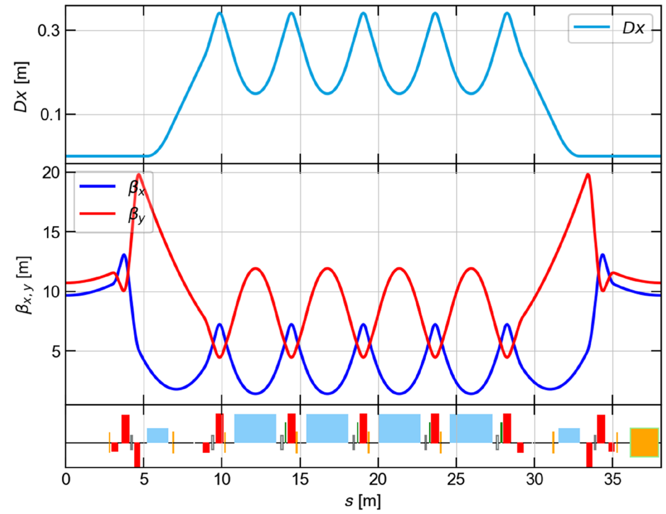

FIG. 11. A classical MBA cell of the DESY booster.

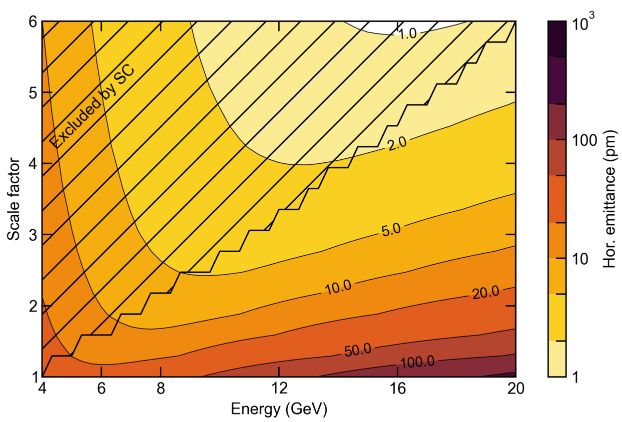

FIG. 10. Achievable emittances as a function of beam energy and lattice scaling factor f for a small coupling $\kappa = 0.1$ in an H6BA lattice with damping wigglers. The wigglers decrease the natural emittance ϵ_0 by a factor of 2.15. Equilibrium emittance is defined by the balance of SR, QE, and IBS. A factor of 10 bunch lengthening by a harmonic rf system is assumed. The hatched area denotes the parameter space unavailable due to the space charge tune spread, $|\Delta\nu_y^{\mathrm{SC}}| > 0.5$. Bunch charge is 1 nC.

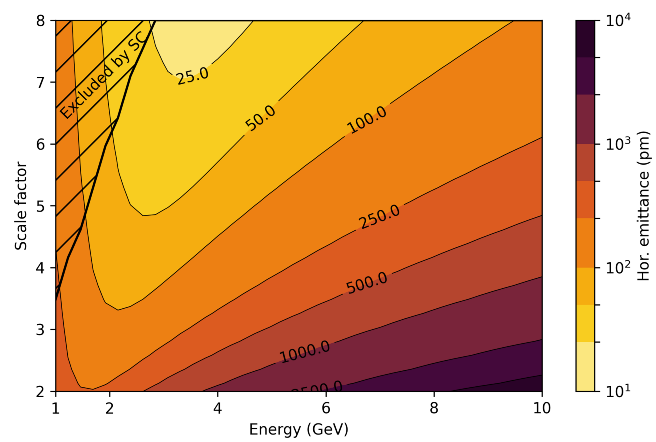

FIG. 12. Achievable emittances as a function of beam energy and lattice scaling factor f for a small coupling $\kappa = 0.01$ in an MBA lattice based on DESY IV. Equilibrium emittance is defined by the balance of SR, QE, and IBS. A factor of 10 bunch lengthening by a harmonic rf system is assumed. The hatched area denotes the parameter space unavailable due to the space charge tune spread, $|\Delta\nu_y^{\mathrm{SC}}| > 0.5$. Bunch charge is 1 nC.

the effect of space charge more prominent: it now excludes a comparatively larger area of parameter space.

The second example is the MBA lattice of the planned DESY IV booster synchrotron (see Fig. 11). It has a 304 m circumference, is based on eight 6-bend MBA cells, and has a natural emittance of 20 nm at 6 GeV. When scaled to a lower energy and shorter cell size, it is comparable to low-energy light sources such as MAX IV [2]. We assumed a bunch charge of 1 nC, which corresponds to 500 mA of stored current with all rf buckets filled. We observe a qualitative similarity with the H6BA case (Fig. 12). As expected, due to a smaller circumference, a significantly shorter cell is required to reach a low emittance, and space charge exclusion is less pronounced.

[1] D. Einfeld, M. Plesko, and J. Schaper, First multi-bend achromat lattice consideration, J. Synchrotron Radiat. **21**, 856 (2014).

[2] S. C. Leemann, A. Andersson, M. Eriksson, L.-J. Lindgren, E. Wallén, J. Bengtsson, and A. Streun, Beam dynamics and expected performance of Sweden's new storage-ring light source: MAX IV, Phys. Rev. ST Accel. Beams **12**, 120701 (2009).

[3] H. N. Chapman, Fourth-generation light sources, IUCrJ **10**, 246 (2023).

[4] P. Raimondi *et al.*, The extremely brilliant source storage ring of the European Synchrotron Radiation Facility, Commun. Phys. **6**, 82 (2023).

[5] Y.-C. Chae, H.-C. Chao *et al.*, PETRA IV: The ultralow-emittance source project at DESY, J. Synchrotron Radiat. **25**, 1277 (2018).

[6] C. Schroer, R. Roehlsberger, E. Weckert, R. Wanzenberg, I. Agapov, R. Brinkmann, and W. Leemans, PETRA IV: Upgrade of PETRA III to the ultimate 3D x-ray microscope, Conceptual Design Report, Deutsches Elektronen-Synchrotron DESY, Hamburg, 2019, p. 259: illustrations, diagrams, https://bib-pubdb1.desy.de/record/426140/.

[7] M. Migliorati, L. Palumbo, and M. Zobov, Bunch length control in DAΦNE by a higher harmonic cavity, Nucl. Instrum. Methods Phys. Res., Sect. A **354**, 215 (1995).

[8] S. A. Antipov, V. Gubaidulin, I. Agapov, E. C. Cortés García, and A. Gamelin, Space charge effects in fourth-generation light sources: The PETRA IV and SOLEIL II cases, Phys. Rev. Accel. Beams **28**, 024401 (2025).

[9] I. Agapov, S. Antipov, R. Bartolini, R. Brinkmann, Y. Chae, E. Cortes-Garcia, D. Einfeld, T. Hellert, M. Huening, M. Jebramcik *et al.*, Beam dynamics performance of the proposed PETRA IV storage ring, arXiv:2408.07995.

[10] P. Raimondi and S. M. Liuzzo, Toward a diffraction limited light source, Phys. Rev. Accel. Beams **26**, 021601 (2023).

[11] M. Sands, The physics of electron storage rings: An introduction, Conf. Proc. C **6906161**, 257 (1969), https://inspirehep.net/literature/60854.

[12] A. Wolski, Low-emittance storage rings, arXiv:1507.02213.

[13] H. Wiedemann, Particle accelerator physics, in *Graduate Texts in Physics*, 4th ed. (Springer, Cham, 2015), pp. 441–446, 459–464.

[14] W. Guo, S. L. Kramer, S. Krinsky, Y. Li, B. Nash, and T. Tanabe, NSLS-II lattice optimization with damping wigglers, in *Proceedings of the Particle Accelerator Conference (PAC 09), Vancouver, Canada* (2010), TU5RFP008, https://inspirehep.net/literature/1378450.

[15] W. Decking and R. Brinkmann, Space charge problems in the TESLA damping ring, in *Proceedings of the 7th European Particle Accelerator Conference (EPAC 2000), Vienna, Austria* (2000), pp. 1024–1026, https://inspirehep.net/literature/538611.

[16] A. Xiao, M. Borland, L. Emery, Y. Wang, and K. Y. Ng, Direct space charge calculation in elegant and its application to the ILC damping ring, Conf. Proc. C **070625**, 3456 (2007).

[17] G. Rumolo, J. B. Jeanneret, Y. Papaphilippou, and D. Quatraro, Collective effects in the CLIC damping rings, Conf. Proc. C **0806233**, MOPP049 (2008), https://inspirehep.net/literature/794590.

[18] M. Zampetakis, F. Antoniou, F. Asvesta, H. Bartosik, and Y. Papaphilippou, Interplay of space charge, intrabeam scattering, and synchrotron radiation in the compact linear collider damping rings, Phys. Rev. Accel. Beams **27**, 064403 (2024).

[19] M. Venturini and K. Oide, Direct space charge effects on the ILC damping rings: Task force report, 10.2172/889308 (2006).

[20] S. Antipov, E. C. Cortés García, and I. Agapov, Space charge limit for light sources, in *Proceedings of the IPAC-2025* (JACoW, Geneva, Switzerland, 2025), MOPS035.

[21] R. Bartolini, Touschek and intrabeam scattering in ultralow emittance storage rings, in *Proceedings of the IPAC-2022* (JACoW, Geneva, Switzerland, 2022), MOIYSP2.

[22] K. L. F. Bane, A simplified model of intrabeam scattering, in *Proceedings of the 8th European Particle Accelerator Conference (EPAC-2002), Paris, France* (2002), pp. 1443–1445, https://inspirehep.net/literature/587892.

[23] A. Piwinski, Intra-beam-scattering, in *Proceedings of the 9th International Conference on High-Energy Accelerators (HEACC 1974), Stanford, California* (1974), pp. 405–409, https://inspirehep.net/literature/94147.

[24] K. L. F. Bane, An accurate, simplified model of intrabeam scattering, arXiv:physics/0205058.

[25] K.-J. Kim, Brightness, coherence and propagation characteristics of synchrotron radiation, Nucl. Instrum. Methods Phys. Res., Sect. A **246**, 71 (1986).

[26] R. P. Walker, Undulator radiation brightness and coherence near the diffraction limit, Phys. Rev. Accel. Beams **22**, 050704 (2019).

[27] E. J. Jaeschke, S. Khan, J. R. Schneider, and J. B. Hastings, *Synchrotron Light Sources and Free-Electron Lasers: Accelerator Physics, Instrumentation and Science Applications*, 1st ed. (Springer International Publishing, Cham, 2016).

[28] G. Geloni, S. Serkez, R. Khubbutdinov, V. Kocharyan, and E. Saldin, Effects of energy spread on brightness and coherence of undulator sources, J. Synchrotron Radiat. **25**, 1335 (2018).

[29] T. Tanaka, Major upgrade of the synchrotron radiation calculation code SPECTRA, J. Synchrotron Radiat. **28**, 1267 (2021).

[30] A. Vannozzi, D. Alesini, C. Sanelli, and C. Vaccarezza, New tunable high gradient permanent magnet quadrupole

for plasma wake field acceleration at SPARC_LAB, J. Phys. Conf. Ser. **1596**, 012009 (2020).

[31] P. Winkler *et al.*, Active energy compression of a laser-plasma electron beam, Nature (London) **640**, 907 (2025).

[32] S. A. Antipov *et al.*, Design of a prototype laser-plasma injector for an electron synchrotron, Phys. Rev. Accel. Beams **24**, 111301 (2021).

[33] S. Posen *et al.*, High gradient performance and quench behavior of a verification cryomodule for a high energy continuous wave linear accelerator, Phys. Rev. Accel. Beams **25**, 042001 (2022).

[34] J.-F. Chen *et al.*, Ultra-high quality factor and ultra-high accelerating gradient achievements in a 1.3 GHz continuous wave cryomodule, Nucl. Sci. Tech. **36**, 25 (2025).

[35] I. Agapov *et al.*, Other science opportunities at the FCC-ee, Technical Report No. CERN-FCC-ACC-2025-0005, CERN, Geneva, 2025, https://cds.cern.ch/record/2928809?ln=en.